Experimental correlations for oscillatory-flow friction and heat transfer in circular tubes with tri-orifice baffles

J. Muñoz-Cámara[a,*], J.P. Solano[a], J. Pérez-García[a]

[a] *Dep. Ingeniería Térmica y de Fluidos, Universidad Politécnica de Cartagena Campus Muralla del Mar (30202) Cartagena, Spain*

doi: https://doi.org/10.1016/j.ijthermalsci.2020.106480

Abstract

Experimental results of isothermal pressure drop and convective heat transfer coefficient are presented for a smooth tube with tri-orifice baffle inserts, under net and oscillatory flow conditions. Using propylene-glycol as working fluid, net Reynolds numbers in the range $Re_n = 10 - 600$ are reproduced, allowing to describe Fanning friction factor in the laminar, transitional and turbulent regimes, with an onset of transition at $Re_n \approx 100$ in steady state conditions. Oscillatory Fanning friction factor for $20 < Re_{osc} < 200$ is also reported, based on the maximum oscillatory pressure drop obtained by statistical fitting of the signal. Nusselt number under uniform heat flux conditions is obtained for superimposed net and oscillatory flows in the ranges $10 < Re_n < 600$ and $10 < Re_{osc} < 440$, with Prandtl number in the range $190 < Pr < 470$. The existence of buoyancy effects in steady-state conditions and its vanishing with oscillations is analysed. The oscillatory flow promotes a 4-fold increase of heat transfer for $Re_n < 20$. For $Re_n > 100$, the effect of

*Corresponding author
Email address: `jose.munoz@upct.es` (J. Muñoz-Cámara)

the flow oscillation on heat transfer enhancement is negligible.

Keywords: oscillatory baffled reactors, multiorifice baffles, transitional flow, heat transfer enhancement, baffled tube

Nomenclature

A_h	heat transfer area (m^2), $\pi D L_h$
c_p	specific heat (J/(kg·K))
d	orifice diameter (m)
D	tube inner diameter (m)
D_{eq}	equivalent diameter (m), $D/\sqrt{n}$
f	oscillation frequency (Hz)
k	thermal conductivity (W/(m·K))
l	cell length (m)
L_h	heated length (m)
L_p	distance between pressure ports (m)
$\dot{m}$	mass flow rate (kg/s)
q_{net}	heat generated by Joule effect (W)
q_{loss}	heat loss (W)
n	number of orifices (-)
S	open area (-), $(n \cdot d/D)^2$
T	temperature (°C)
t	time (s)
U_n	mean velocity of the net flow (m/s), based on D
x	axial distance from the start of the heated area (m)
x_0	oscillation amplitude, center to peak (m)

Δp	net pressure drop (Pa)
Δp_{max}	maximum pressure drop under oscillatory flow conditions (Pa)

Dimensionless groups

Re_n	net Reynolds number, $\rho U_n D/\mu$
Re_{osc}	oscillatory Reynolds number, $\rho(2\pi f x_0)D/\mu$
Ψ	velocity ratio, Re_{osc}/Re_n
Pr	Prandtl number, $\mu c_p/k$
f_n	net Fanning friction factor, $\frac{\Delta p}{2\rho(U_n)^2}\frac{D}{L}$
f_{osc}	oscillatory Fanning friction factor, $\frac{\Delta p_{max}}{2\rho(2\pi f x_0)^2}\frac{D}{L}$
Nu	Nusselt number, hD/k

Greek symbols

μ	dynamic viscosity (kg/(m·s))
ρ	fluid density (kg/m^3)
σ	standard deviation
τ	oscillation period (s)

Subscripts

b	bulk
cr	start of the transitional flow regime
in	inlet
j	section number
k	circumferential position number
qt	start of the quasi-turbulent flow regime

t	start of the turbulent flow regime
wi	inner wall

1. Introduction

The use of oscillatory flow as a general purpose means for heat transfer enhancement has attracted the interest of numerous researchers in the last years, including industrial applications such as heat exchangers [1, 2], Stirling engine regenerators [3] or chemical reactors [4]. The latter have found potential improvements over conventional reactors with the development of the oscillatory baffled reactors (OBRs), which are the focus of this study.
OBRs are based on the superposition of an oscillatory flow to a very low net flow in a tube with inserted geometries, allowing simultaneously for high residence times, high radial mixing and low axial dispersion. These devices have been a focus of many studies during the last decades due to their remarkable advantages in comparison to the conventional stirred tanks. Some of these positives are the low shear rate and the easy scale-up [5], the continuous throughput and the enhanced mixing [6] and heat transfer [7, 4].
Despite of this, there is a significant issue related to its scalability, because the oscillation frequency must be reduced in order to keep the similarity for a pilot scale reactor. This reduction can imply a poor mixing and an extremely low shear rate [5]. Two alternatives have been proposed to solve this problem: the first is a parallel tubes arrangement [8], which makes easier the scale-up, but ensuring a uniform distribution of the oscillation is a demanding task; another solution is the multi-orifice baffled reactor, whose mass transfer behavior is

quite similar to a series of parallel one-orifice baffled tubes [9]. For the latter case, the concept of equivalent diameter is introduced, $D_{eq} = D/\sqrt{n}$, so that, from a point of view of the mixing rate, a multi-orifice baffled tube with a diameter D and n holes can be considered equivalent to a one-orifice baffled reactor with a diameter D_{eq}.

The literature review shows that the multi-orifice baffled reactors are the prevailing solution, as can be deduced by the significant number of current studies about their potential applications. For instance, some studies have proved experimentally its better performance in liquid-gas mass transfer in comparison to other designs [10], its suitability for applications of CO_2 dissolution [11], crystallization [12], or ozonation [13] and transesterification [14] processes.

In spite of its applicability, there is a lack of studies regarding its fluid mechanics and thermohydraulic behavior. Smith [15] studied qualitatively the flow pattern in a one-orifice and a multi-orifice (37 holes) baffled tube with the same equivalent diameter. The results showed that the flow behavior was similar for both geometries, at the expense of a lower net Reynolds number in the multi-orifice case, and how the flow becomes asymmetric for a net Reynolds number equal to 100 for the multi-orifice baffle, approximately half of the value for a one-orifice baffle. The flow visualization and RTD analysis conducted by González-Juárez et al. [16] confirmed the reduction of dead zones and the achievement of a more uniform mixing when the number of orifices is increased for the same flow conditions ($Re_n = 50$, $Re_{osc} = 800$, based on the tube diameter). They also obtained the net friction factor and the power consumption related to the oscillatory flow, showing that both magnitudes increase when the number of orifices is increased. Nogueira et al. [17] studied the oscillatory flow in a tri-orifice baffled tube for two oscillatory Reynolds numbers (based on the equivalent tube diameter), $Re_{osc} = 600$ and 1200. They observed the mixing uniformity, with special attention to the mechanisms of the vortex rings generation at each orifice and the 3D complexity of the generated structures.

Focusing on the heat transfer, while one-orifice reactors have been studied with some detail under static [18] and dynamic conditions [7, 19], there are only a reduced amount of data for multi-orifice baffles and are limited to operation in batch mode and a reduced range of oscillatory Reynolds numbers [20], so there are no available correlations for multi-orifice baffles or studies which consider the net flow effect nor the Prandtl number. In addition, while it is relatively easy to find recent studies about mixed convection in smooth tubes [21, 22], that it is not the case for enhanced geometries as baffled tubes. So, there are no published results that can serve as a guideline for determining when the stratification of the flow can appear. This is a remarkable point because OBRs are designed to work at very low net Reynolds numbers, where the mixed convection could play a significant role.

Thus, the main goal of this paper is to provide an experimental correlation for heat transfer in tubes with equally spaced tri-orifice baffles. The tested geometry is based on the recommended parameters for the design of multi-orifice baffled reactors [15]. The cross-sectional open area is $S = 0.25$ and the interbaffle spacing is $l = 1.5/D_{eq}$. The tests are performed under uniform heat flux conditions, covering a wide range of flow conditions $10 < Re_n < 600$, $170 < Pr < 480$, $50 < Re_{osc} < 440$. Additionally, pressure drop under net and oscillatory flow conditions is studied and a correlation for the corresponding friction factors is given.

2. Experimental test rig

2.1. Geometry

The relevant parameters of the tested geometry are shown in Figure 1. The orifice diameter of the three orifices is 9.2 mm, in a tube with inner diameter D=32 mm, which yields a cross-sectional open area $S = 0.25$. The equivalent diameter is 15.5 mm approximately, and the interbaffle spacing is consequently 27.6 mm, following the criterion $l = 1.5_{eq}$. The orifice center is placed at one half radius from the tube center and the angular position is equally distributed at 120°. The 1 mm thick baffles are made of PEEK plastic to avoid the electrical conduction from the tube wall. A central rod of 3 mm diameter is used to connect the baffles.

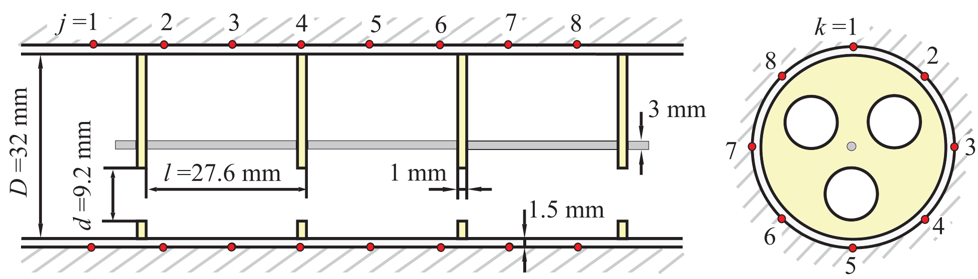

Figure 1: Baffle geometry and thermocouple arrangement in the test section.

2.2. Thermal-hydraulic test rig

Figure 2 shows the experimental arrangement used to study the heat transfer and pressure drop in these devices. The main fluid (pure propylene-glycol) is stored in an open reservoir tank (1), whose temperature is controlled by an independent circuit (more information about this auxiliary circuit can be found in [18]). A stirring device (14) ensures that the fluid temperature in the tank is homogeneous. The fluid is pumped by a train of three variable-speed gear pumps (2), which ensure that the net flow rate variations due to the pressure fluctuations produced by the fluid oscillation are minimum. These three pumps can work individually or simultaneously. A Coriolis effect flowmeter (3) measures the net mass flow rate. The test section consists of 2 m long 316L stainless steel horizontal tube (32 mm inlet diameter, 1.5 mm thick) where 56 tri-orifice baffles are inserted (5).

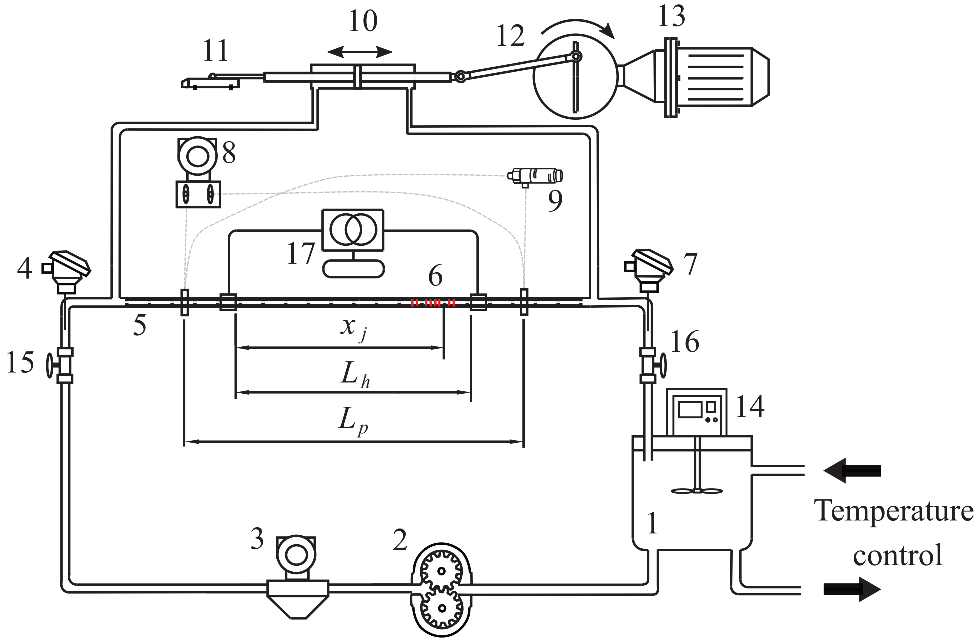

Figure 2: Experimental set-up. (1) Reservoir tank, (2) Pumping system, (3) Coriolis flowmeter, (4) PT-100 Class B 1/10 DIN temperature sensors, inlet, (5) Baffles, (6) Wall thermocouples, (7) PT100, outlet, (8) Differential pressure transducer, (9) Fast response time pressure sensor, (10) Double acting cylinder, (11) Displacement sensor, (12) Crank and connecting rod, (13) Gear reducer, (14) Motor, (15,16) Manual valve, (17) Autotransformer

The oscillatory flow in the test section is provided by the displacement of a hydraulic cylinder (10), whose time-dependent position is measured by a magnetostrictive position transducer (11). The hydraulic cylinder is driven by a crank and connecting rod arrangement (12). The oscillation frequency is set by adjusting the rotation frequency of the motor (13). The oscillation amplitude is set by moving the connecting rod along a disk slot. The position is set to ensure an oscillation amplitude equal to 9.2 mm, which is the orifice the diameter, $x_0 = d$. This value is used to ensure the flow similarity with a one-orifice baffled tube [9].

For the net pressure drop experiments, a set of differential pressure transducers (8), model SMAR LD301, ensures that the differential pressure drop between two ports (at a distance L =1.296 meters) is accurate enough along the whole range of flow rates tested. The ranges of the transducers are: 0-10 mbar, 0-50 mbar, 5-500 mbar and 22-2500 mbar.

For the measurement of the pressure drop related to the oscillatory flow, four fast response piezoresistive pressure sensors (9) are used. Two of them are bidirectional and differential, model KISTLER 4264A, with ranges $\pm$100 mbar and $\pm$1bar; and two are absolute, model KISTLER 4262A, with ranges 0-7 bar and 0-10 bar.

The pressure drop under oscillatory flow is measured without net flow. To avoid the effect of the rest of the circuit, the loop with oscillatory flow is isolated by closing the manual valves (15 and 16). As it was reported by Baird and Stonestreet [23], under high oscillating frequencies the high pressure drop can lead to cavitation in the oscillating device. So, previously to the valves closing, the system is pressurized at 3 bar (relative pressure). All these tests are done under isothermal conditions.

For the heat transfer experiments, the tube is heated by means of Joule effect, applying an AC current through the tube shell, which acts as an electrical resistance. The voltage is applied by a variable autotransformer (17), which allows to control the current intensity and so, the temperature difference between the wall and the fluid. This temperature difference is adjusted to achieve a high enough value that reduces the error mainly associated to the wall temperature measurement. The wall temperatures (6) are measured, by T-type thermocouples, at a distance from the beginning of the heating section which is long enough to avoid entrance effects. The test section is insulated with an elastomeric material, reducing the thermal losses. The power absorbed by the test section is calculated from the voltage and the intensity. The fluid inlet and outlet temperatures are measured by RTD (Resistance Temperature Detector) sensors (4,7).

The temperature at the inlet of the circuit is adjusted using the temperature control loop to achieve the desired temperature at the test section. Three sets of experiments are conducted for three different temperatures: 20 °C, 26 °C and 40 °C, corresponding to Prandtl numbers: 470, 340 and 190, respectively.

In order to measure the wall temperature properly, two aspects should be taken into account: 1) the axial variation of the velocity profile should have a significant role on the heat transfer coefficient along a cell tank, i.e., the distance between consecutive baffles; 2) the flow stratification could lead to a significant circumferential gradient of the wall temperature at the same cross section. To solve both considerations, 64 thermocouples are placed at eight different axial sections and eight circumferential positions at each section (see Figure 1).

The signals from the fast response pressure sensors and the position transducer are acquired with a high speed acquisition card model USB-6001, and they are sampled with a frequency of 2.8 kHz for each channel. The rest of the measurements are acquired by two dataloggers, models Agilent 34970A and 34972A, with a frequency of 0.1 Hz.

2.3. Data reduction

The net flow is characterised by the net Reynolds number, which is calculated using Eq. 1.

$$Re_n = \frac{4\ \dot{m}}{\pi\ \mu\ D} \tag{1}$$

To describe the oscillatory flow, the oscillatory Reynolds number, Re_{osc}, is used (Eq. 2).

$$Re_{osc} = \frac{\rho\ (2\pi f x_0)\ D}{\mu} \tag{2}$$

where f and x_0 are, respectively, the frequency and amplitude of the oscillatory flow. Both are measured using the signal of the displacement sensor. An additional parameter, the velocity ratio, $\Psi = Re_{osc}/Re_n$, is used to indicate the significance of the oscillatory flow in comparison to the net flow. The Fanning friction factors associated to the net flow and the oscillatory flow are calculated according to Eq. 3 and 4, respectively.

$$f_n = \frac{\Delta p}{2\rho (U_n)^2} \frac{D}{L} \tag{3}$$

$$f_{osc} = \frac{\Delta p_{max}}{2\rho (2\pi f x_0)^2} \frac{D}{L} \tag{4}$$

where Δp is the pressure drop along the length of the test section, L_p. As can be observed, the oscillatory Fanning friction factor is defined similarly to the net Fanning friction factor, but the maximum of the instantaneous pressure drop, Δp_{max}, and the maximum oscillatory velocity, $2\pi f x_0$, are used instead of the mean pressure drop and the net flow velocity.

Prior to the heat transfer measurements, the wall temperature measurements should be corrected because the thermocouples are not perfectly attached to the wall. To correlate the measured and the real temperature, a set of calibration experiments is done. For each experiment, steady-state isothermal conditions at very high flow rates are achieved, this allows us to calculate the real outside wall temperature considering the steel tube and insulation resistance and the internal and external convection coefficients. The effect of the internal convection coefficient is negligible due to the high value in comparison to the rest of the terms.

The local Nusselt number at each cross section, j, (see Figure 1) is computed as:

$$\bar{Nu}_j = \frac{(q_{net} - q_{loss})/A_h}{\bar{T}_{wi,j} - T_{b,j}} \cdot \frac{D}{k} \tag{5}$$

where q_{net} is the heat generated by Joule effect, calculated as the voltage times the electric current, and q_{loss} is the heat loss, calculated assuming natural convection with the surroundings using the correlation proposed by Churchill and Chu [24]. A_h is the heat transfer area.

$\bar{T}_{wi,j}$ is the peripherally averaged inner wall temperature at the j section. It is derived from the outer wall temperature using a one-dimensional numerical model which solves the radial heat conduction equation in the tube wall, considering internal heat generation.

$T_{b,j}$ is the bulk fluid temperature at the section j. It was calculated by considering a linear variation with the axial direction, since the heat was added uniformly along the tube length:

$$T_{b,j} = T_{b,in} + \frac{q_{net} - q_{loss}}{\dot{m}\ c_p} \cdot \frac{x_j}{L_h} \tag{6}$$

where $T_{b,in}$ is the fluid temperature at the inlet of the test section. x_j is the axial distance between the test section j and the point where the tube heating starts.

The circumferential average Nusselt number is corrected by the factor $(\mu_{wi}/\mu_b)^{0.11}$ to account for the change in the physical properties due to the radial temperature gradient [25]. Finally, the mean Nusselt number is obtained averaging the Nusselt number for the eight axial sections.

Once the results were obtained, an uncertainty estimation was done, following the guidelines described in [18]. The maximum and mean uncertainties values based on a 95% confidence level are summarized in Table 1.

Variable	Max. uncertainty	Mean uncertainty
x_0	7.2%	7.2%
Re_n	7.3%	3.9%
Re_{osc}	6.6%	4.9%
Pr	4.7%	3.5%
f_n	10.3	3.2%
f_{osc}	7.2%	5.1%
Nu	10.4%	7.4%

Table 1: Uncertainties of the relevant variables

3. Thermal-hydraulic results

3.1. Pressure drop for net-flow conditions

In this subsection, the results related to pressure drop under net flow conditions are provided for the range $10 < Re_n < 600$. Figure 3 (a) shows the Fanning friction factor as a function of the net Reynolds number, and, as a reference, the experimental correlation for the friction factor of a one-orifice baffled geometry [18].

As can be observed, the Fanning friction factor for the tri-orifice baffled tube is significantly higher than for a one-orifice baffled tube. In order to compare both geometries, two aspects should be considered: the change of the geometry and the reduction of the interbaffle spacing for the same tube inner diameter. In this case, the main factor in the pressure drop increase is the interbaffle spacing, which results in 70% more baffles per unit of length when the number of orifices is increased from one to three. There is also a slight effect of the geometry. As an example, a calculation of the pressure drop per single baffle shows that it is 6% lower for the one-orifice baffles at $Re_n = 400$.

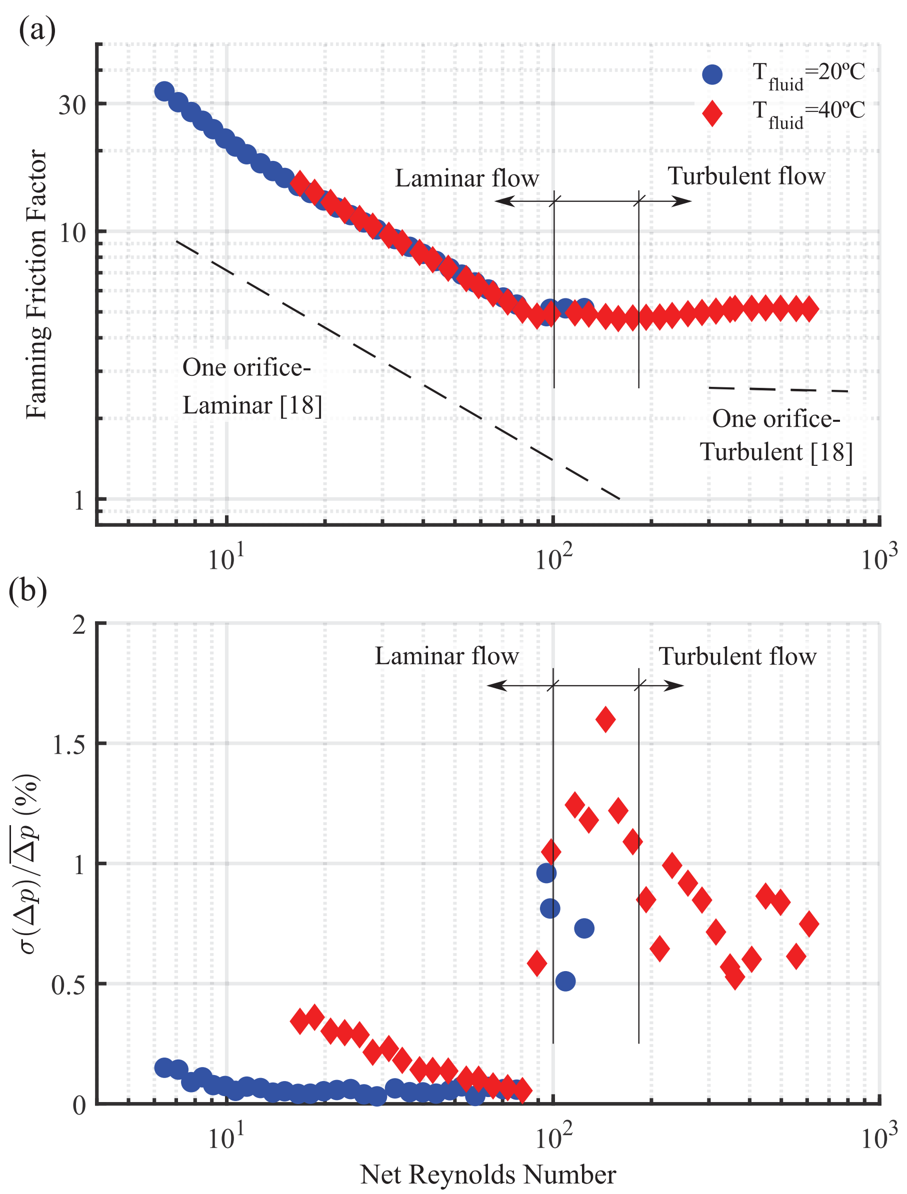

Figure 3: (a) Fanning friction factor *vs* net Reynolds number for two fluid temperatures (b) Standard deviation of pressure drop measurements *vs* net Reynolds number for two fluid temperatures.

To ease the detection of the transitional region, the pressure drop fluctuations (divided by the average pressure drop) are plotted as a function of the net Reynolds number in Figure 3 (b), as it was proposed by Meyer and Olivier [26]. For $Re_n < 90$ the pressure drop fluctuations have low values and small variations with the net Reynolds number. In a perfect laminar flow this fluctuation should be zero, but the electrical noise and the slight flow rate fluctuations due to the gear pump can be noticeable. Above $Re_n = 90$ there is a sharp increase in the pressure drop fluctuations, with a significant variation with the net Reynolds number, setting the onset of the transitional flow regime. A slight decrease in the pressure fluctuations is observed when the net Reynolds number is in the turbulent flow region. This is the general trend that was also observed by the authors for several enhanced tubes [26]. Everts and Meyer [27] proposed several criteria to detect the limits between the different flow regimes: laminar, transitional, quasi-turbulent and turbulent. The authors established the onset of the transitional flow regime, from heat transfer results, by locating the point where $\delta Nu/\delta Re = 0$. Similarly, the onset of the transitional flow regime is found from our pressure drop results, detecting the point where: $\delta f_n/\delta Re = 0$. This allowed us to detect the critical value: $Re_{cr} = 110$.

However, from Figure 3 (a), it is quite noticeable the difference between the trends of the Fanning friction factor for a tri-orifice baffled tube and a smooth tube during the transitional flow regime. So, the same methodology could not be successfully be applied to the results to detect the onset of the quasi-turbulent and the turbulent flow regime. Instead, the value for the onset of the turbulent flow regime obtained from the heat transfer results (see section

3.2) was used: $Re_t = 183$.

Once the limits have been defined, two correlations are proposed for the laminar and turbulent flow regimes (Eq. 7 and 8). They adjust all the experimental measurements within 10%.

$$f_n = 130.8\ Re_n^{-0.761} \qquad 6 < Re_n < 110 \tag{7}$$

$$f_n = 3.22\ Re_n^{0.076} \qquad 183 < Re_n < 600 \tag{8}$$

3.2. Heat transfer for net-flow conditions

In spite of the fact that these devices are not designed to work with net, steady-state flow, a study of the net Reynolds number on heat transfer is interesting to corroborate the onset of the transitional flow regime (because they are designed to work at very low net Reynolds numbers) and quantify the effect of the Prandtl number on the heat transfer rate.

Figure 4 shows the Nusselt number as a function of the net Reynolds number for three different Prandtl numbers. To show the coherence of the results, the Nusselt number is multiplied by the factor $Pr^{-0.285}$, removing the effect of the Prandtl number. The exponent -0.285 for the Prandtl number has been obtained previously by means of a statistical fitting.

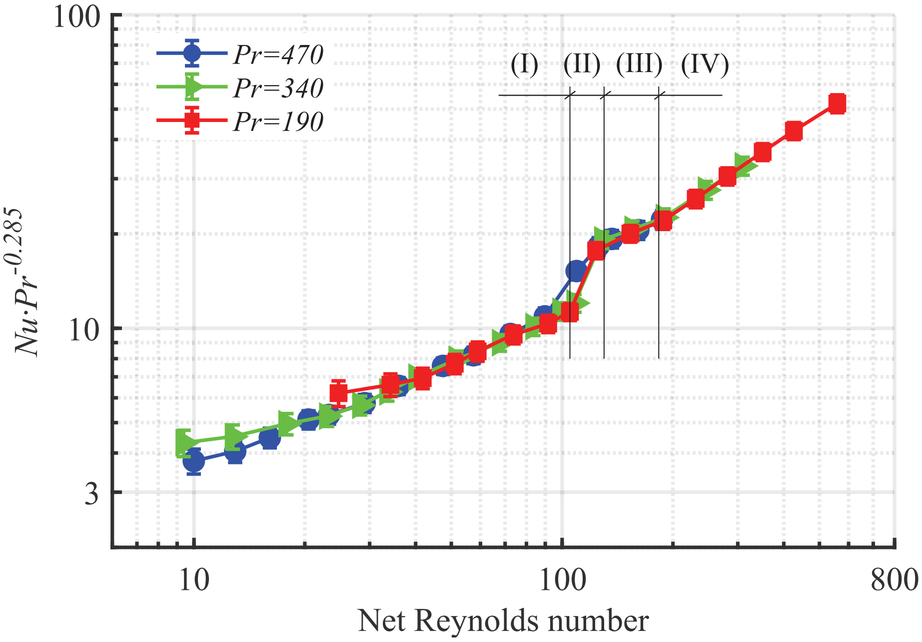

Figure 4: Nusselt number *vs* Reynolds number for the three Prandtl numbers tested

Following the general criteria described by Everts and Meyer [27], four different regions are observed (see Figure 4): laminar (I), transitional (II), quasi-turbulent (III) and turbulent (IV). The end of the laminar region is marked by a sudden rise of the Nusselt number above $Re_{cr} = 105$. This limit was obtained by detecting the point where $\delta Nu/\delta Re$ is maximum, i.e., the variation of the slope in Figure 4 is higher. This value is similar to the limit obtained from the pressure measurements, $Re_n = 110$. The difference can be justified by the thermal effects on the onset of the transition.

The quasi-turbulent flow regime, from $Re_{cr} = 105$ to $Re_{qt} = 130$, is characterized by a high increase in the Nusselt number and its middle point corresponds to the point where $\delta^2 Nu/\delta Re^2 = 0$ [27]. On the other hand, the onset of the turbulent region cannot be identified using known correlations for the turbulent flow regime as the authors did. As an alternative, an iterative algorithm is implemented, based on the linear method used by Meyer and Abolarin [28]. For each net Reynolds number tested above the onset of the quasi-turbulent flow regime, two statistical fittings are accomplished to fit two lines to the experimental measurements, below that given Reynolds number and above it. There is a unique net Reynolds number which reduces the overall fitting error to a minimum. This last net Reynolds number is considered as an optimum to separate and fit both regions. Finally, the intersection point of the fitted lines, $Re_t = 183$, is taken as the onset of the turbulent flow regime.

The laminar and turbulent regions are fitted to correlations (Eq. 9 and 10). Since the measurement error for each point is significantly different, a weighted nonlinear fitting has been considered appropriate. Thus, the term corresponding to a given measurement, used in the mean squared algorithm for the statistical fitting, is weighted proportionally to the inverse of the estimated error [29].

$$Nu = 1.08\ Re_n^{0.501}\ Pr^{0.285} \qquad 10 < Re_n < 105; 190 < Pr < 470 \tag{9}$$

$$Nu = 0.43\ Re_n^{0.756}\ Pr^{0.285} \qquad 183 < Re_n < 600; 190 < Pr < 470 \tag{10}$$

A comparison between the predicted values and the experimental results shows that more than 90% of the experimental data are in a range of ± 10% from the proposed correlation.

During the measurements, a notable temperature difference between the thermocouples placed at the upper and the lower point of the tube was observed. As an example, a representation of the circumferential wall temperatures in a section measured by the corresponding eight thermocouples is plotted in Figure 5 (b), where a temperature difference ΔT=8.5 °C is found between the bottom and top positions, for a mass flow $\dot{m}$=34 kg/h and a heat flux q"=1.4 kW/m^2.

Consequently, a more detailed study is of interest to determine the effect of the net flow on the flow stratification. To easily characterize the level of flow stratification, the mean difference between the upper ($\bar{T}_{wi,j,1}$) and lower ($\bar{T}_{wi,j,5}$) wall temperatures (see Figure 1) is plotted in Figure 5 (a) for the three Prandtl numbers as a function of the net Reynolds number.

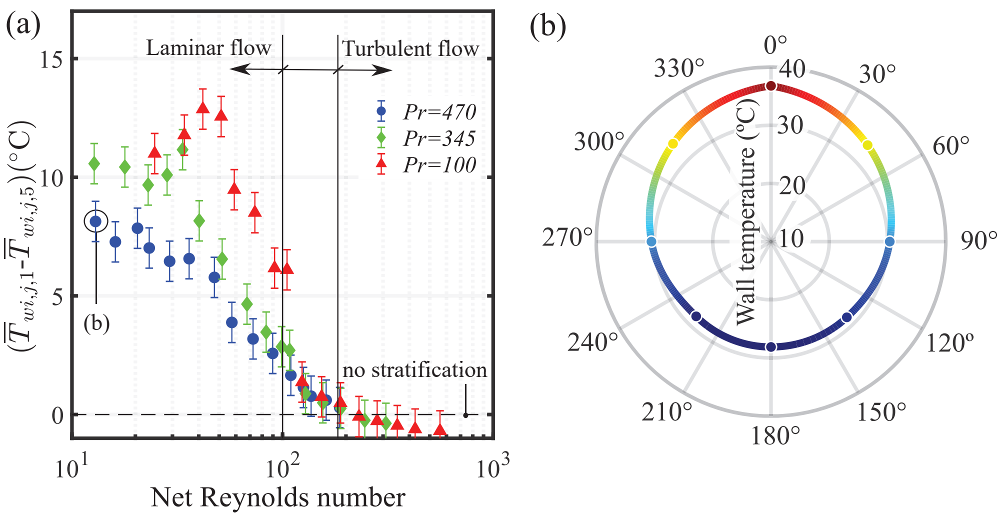

Figure 5: (a) Temperature difference due to the stratification *vs* net Reynolds number for three Prandtl numbers. (b) Measured temperature distribution in a cross section for Re_n = 10, Re_{osc} = 0 and Pr = 470.

From Figure 5 (a), the existence of flow stratification is quite noticeable for $Re_n < 100$ (laminar region) and for the studied range of Prandtl numbers. When the flow becomes transitional above that value, the inertial forces are dominant over the effect of the buoyancy and the temperature stratification is reduced considerably.

3.3. Pressure drop for oscillatory-flow conditions

The data reduction of the pressure drop signal under oscillatory flow is not as straightforward as in the net flow situation. Figure 6 represents the pressure drop at 24 °C and oscillation frequency 3.2 Hz. It can be noticed that the signal is not purely a sinusoidal wave. A clear and repetitive perturbation and the subsequent attenuation is observed during the positive and negative parts of the cycle. This was observed to occur at the end of the piston strokes, when a sudden acceleration takes place due to the imperfect movement of the piston.

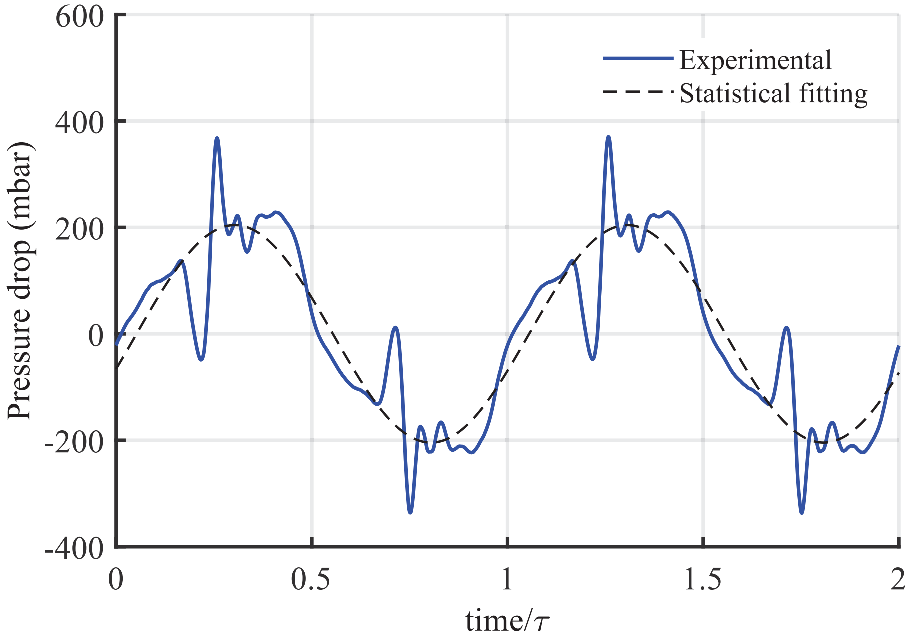

Figure 6: Instantaneous experimental pressure drop and statistical fitting *vs* dimensionless time. Fluid temperature=24 °C and f=3.2 Hz.

Despite the mentioned perturbation, the fundamental component of the pressure wave can be observed. The problem now is to consider only the amplitude corresponding to the fundamental wave of the pressure drop, discarding the peaks related to perturbations. As a solution, it was decided to use a nonlinear statistical fitting to the experimental pressure wave. The statistical fitting is plotted with the original signal in Figure 6.

The amplitude of the adjusted pressure wave is used as the maximum pressure drop, Δp_{max}, for the calculation of the oscillatory Fanning friction factor. This dimensionless number is plotted as a function of the oscillatory Reynolds number in Figure 7. For the sake of comparison, the correlations previously obtained in this work for the net Fanning friction factor are also plotted.

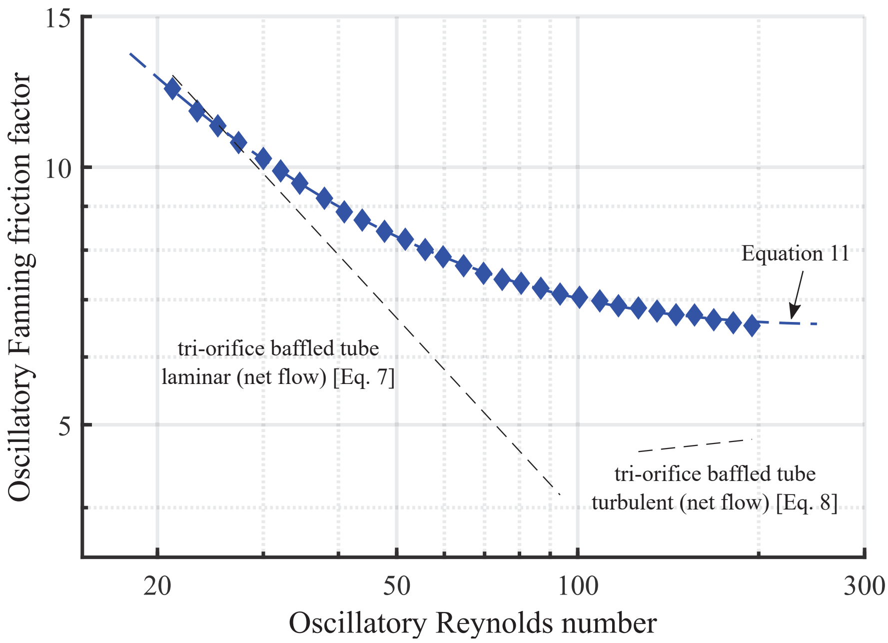

Figure 7: Oscillatory Fanning friction factor *vs* oscillatory Reynolds number. Amplitude, $x_0 = d$.

If the flow could be described as quasi-steady, the curves for the net and the oscillatory Fanning friction would be overlapped. That is what can be observed at very low oscillatory Reynolds numbers, $Re_{osc} < 30$. For higher Re_{osc}, the maximum pressure drop is significantly higher than the value corresponding to the same Reynolds number under steady flow conditions. Additionally, the variation of the slope in the oscillatory Fanning friction factor suggests a change in the flow regime, from laminar unsteady to a more chaotic flow.

The experimental results are adjusted to an empirical correlation (Eq. 11), following the form of a three parameters modified-Ergun's equation [30], commonly used in Stirling engine regenerators [31].

$$f_{osc} = \frac{162}{Re_{osc}} + 3.46\ Re_{osc}^{0.097} \qquad\qquad 20 < Re_{osc} < 200 \tag{11}$$

This correlation fits all the experimental data with a maximum relative error of 2%.

3.4. Heat transfer for oscillatory-flow conditions

In this subsection, the results related to heat transfer with net and oscillatory flow are presented. Figure 8 (a) and (b) represents the Nusselt number as a function of the net Reynolds number for several oscillatory Reynolds number for two different Prandtl numbers.

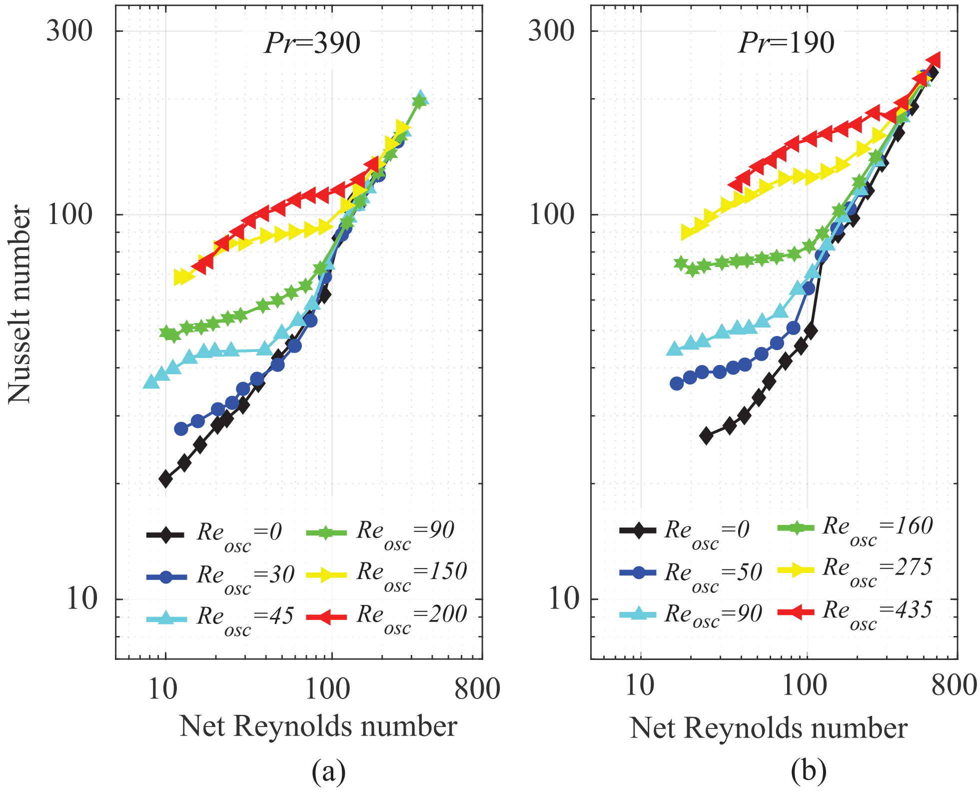

Figure 8: Nusselt number *vs* net Reynolds number for different oscillatory Reynolds numbers. Amplitude, $x_0 = d$. (a) $Pr = 390$ and (b) $Pr = 190$

As can be seen for both Prandtl numbers, the oscillatory flow can introduce a significant heat transfer augmentation in comparison with the only net flow case ($Re_{osc} = 0$). For example, for $Pr = 390$ and $Re_n = 10$, the case with only net flow presents a Nusselt number $Nu \approx 20$, while a value of $Nu \approx 70$ can be achieved superimposing an oscillatory flow with $Re_{osc} = 150$, which means an increase of about 3.5 times.

The significant enhancement in heat transfer when an oscillatory flow is superimposed can be justified by the flow patterns observed experimentally

[17] and numerically [16] in tri-orifice baffles under oscillatory flow conditions. During both the positive and negative parts of the cycle (when there is flow reversal, $Re_{osc}/Re_n < 1$), vortices are generated downstream of the baffles and move along the space between consecutive baffles increasing the mixing and disturbing the boundary layer.

It can be also observed how the net Reynolds number has a slightly positive enhancement effect for a given oscillatory Reynolds number. But the effect is lower than in the only net flow case, as can be deduced from the different slope in the curves with oscillatory flow and the curve with only net flow. Another remarkable effect is the lack of enhancement when the net and oscillatory Reynolds numbers are of the same order of magnitude, i.e. low velocity ratios. This can be explained by the fact that at $Re_{osc}/Re_n < 1$ there is no flow reversal, so vortices are not generated during one half of the cycle, reducing the overall mixing intensity.

The effect of Prandtl number on oscillatory flow heat transfer can be analysed on the basis of single results. For a constant $Re_n = 20$, results for $Pr = 390$ (Figure 8 (a)) and $Re_{osc} = 160$ yield a Nusselt number $Nu = 90$. For $Pr = 190$ (Figure 8 (b)), $Re_n = 20$ and $Re_{osc} = 150$, $Nu = 75$. Taking into account the negligible difference among the two different values of Re_{osc}, an increase of Nusselt number of 20 % is reported for the highest Prandtl number data set. The prediction obtained with the exponent 0.285 obtained to quantify the effect of Prandtl number under net flow conditions would yield a 22.7 % increase on Nusselt number. The small difference between both outcomes, which is below the measurement uncertainty, supports the idea that the Prandt number effect does not change when an oscillatory flow is applied.

A more detailed look at the effect of the oscillatory flow on the stratification is also of high interest. Figure 9 represents the mean difference between the upper and lower wall temperatures as a function of the net Reynolds number for five different oscillatory Reynolds numbers and a Prandtl number $Pr = 190$.

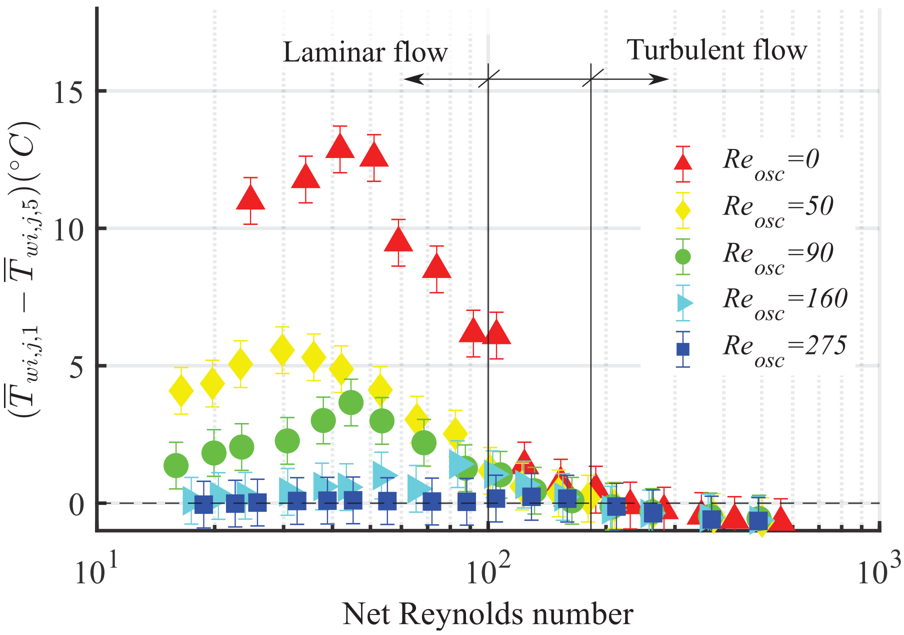

Figure 9: Temperature difference due to the stratification *vs* net Reynolds number for several oscillatory Reynolds numbers ($Pr = 190$)

From Figure 9, a progressive reduction of the flow stratification is observed when the oscillatory Reynolds number is increased. For example, at a $Re_n = 30$ there is a temperature difference of $10^{\circ}C$ when no oscillation is applied, which is reduced up to $5^{\circ}C$ for a $Re_{osc} = 50$ and completely removed at

$Re_{osc} = 160$. This also supports the idea of a high mixing at very low net Reynolds numbers when an oscillatory flow is superimposed.

The goal now is fitting the heat transfer data to an adequate correlation. Previously proposed correlations [7, 19, 32] have tried to consider the steady and the oscillatory results in only one equation. Nevertheless, for the studied range, the existence of three clearly different regions for the steady case makes the process trickier. In addition, it should be considered that a portion of the data does not have usefulness for real applications. Stonestreet and van der Veeken [33] identified the value Ψ=1.8-2 to obtain the optimal residence time distribution. So, it is decided to use only the data with oscillatory flow and a velocity ratio $\Psi > 1$. The Prandtl number exponent is the same as the one previously obtained from the fitting of the net flow data.

$$Nu = 0.412\ Re_n^{0.196}\ Re_{osc}^{0.583}\ Pr^{0.285} \qquad\qquad \Psi > 1 \qquad\qquad (12)$$

The fitting of the correlation (Eq. 12) to the experimental data is plotted in Figure 10. These correlation fits an 87% of the data with a deviation of $\pm$ 10% and all the data with a deviation of $\pm$ 20%.

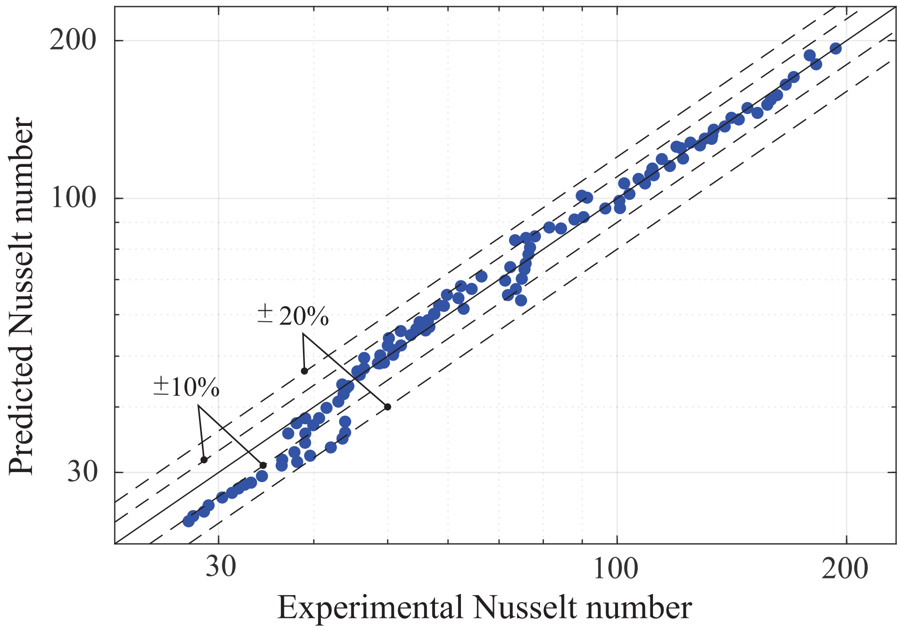

Figure 10: Experimental *vs* predicted Nusselt for the proposed correlation (Eq. 12)

4. Conclusions

- In the absence of oscillation, three different flow regimes have been distinguished: laminar flow regime for $Re_n < 110$, transitional flow regime for $110 < Re_n < 185$ and turbulent flow regime for $Re_n > 185$. A 3-fold increase of friction factor in the laminar regime, with respect to the standard geometry of one-orifice baffle, is reported.

- The superimposition of an oscillatory flow involves a remarkable increase in the heat transfer rate, up to 4 times for very low net Reynolds numbers. However, the heat transfer enhancement effect is negligible for low velocity ratios, $Re_{osc}/Re_n < 1$, especially when the flow becomes turbulent, $Re_n > 100$.

- An influence of Prandtl number on heat transfer in the form $Nu\ \alpha\ Pr^{0.285}$ has been obtained for both net-flow and superimposed oscillatory flow conditions, in the ranges $10 < Re_n < 600$ and $0 < Re_{osc} < 600$ and $190 < Pr < 470$.

- Flow stratification has been observed in the laminar flow region ($Re_n < 100$), and it has been proved that this can be reduced, and even removed, if an oscillation is superimposed to the flow.

Acknowledgements

The authors gratefully acknowledge the financial support of the project DPI2015-661943-P by Ministerio de Economía y Competitividad (MINECO, Spain) and the Fondo Europeo de Desarrollo Regional (FEDER).

5. References

[1] C. Wantha, Effect and heat transfer correlations of finned tube heat exchanger under unsteady pulsating flows, International Journal of Heat and Mass Transfer 99 (2016) 141–148.

[2] W. Kamsanam, X. Mao, A. J. Jaworski, Thermal performance of finned-tube thermoacoustic heat exchangers in oscillatory flow conditions, International Journal of Thermal Sciences 101 (2016) 169–180.

[3] I. Barreno, S. C. Costa, M. Cordon, M. Tutar, I. Urrutibeascoa, X. Gomez, G. Castillo, Numerical correlation for the pressure drop in Stirling engine heat exchangers, International Journal of Thermal Sciences 97 (2015) 68–81.

[4] I. I. Onyemelukwe, B. Benyahia, N. M. Reis, Z. K. Nagy, C. D. Rielly, The heat transfer characteristics of a mesoscale continuous oscillatory flow crystalliser with smooth periodic constrictions, International Journal of Heat and Mass Transfer 123 (2018) 1109–1119.

[5] M. S. R. Abbott, A. P. Harvey, G. Valente Perez, M. K. Theodorou, Biological processing in oscillatory baffled reactors: operation, advantages and potential, Interface focus 3 (1) (2013) 20120036.

[6] N. Xiongwei, G. Siwen, Mass transfer characteristics of a pilot pulsed baffled reactor, Journal of Chemical Technology & Biotechnology 65 (1) (1999) 65–71.

[7] M. R. Mackley, P. Stonestreet, Heat transfer and associated energy dissipation for oscillatory flow in baffled tubes, Chemical Engineering 50 (14) (1995) 2211–2224.

[8] X. Ni, Residence time distribution measurements in a pulsed baffled tube bundle, Journal of Chemical Technology & Biotechnology 59 (3) (1994) 213–221.

[9] K. Smith, M. Mackley, An experimental investigation into the scale-up of oscillatory flow mixing in baffled tubes, Chemical Engineering Research and Design 84 (11) (2006) 1001–1011.

[10] S. M. R. Ahmed, A. N. Phan, A. P. Harvey, Mass transfer enhancement as a function of oscillatory baffled reactor design, Chemical Engineering & Processing: Process Intensification 130 (2018) 229–239.

[11] F. M. Pereira, D. Z. Sousa, M. M. Alves, M. R. Mackley, N. M. Reis, CO2 Dissolution and design aspects of a multiorifice oscillatory baffled column, Industrial & Engineering Chemistry Research 53 (44) (2014) 17303–17316.

[12] A. Laybourn, A. M. López-Fernández, I. Thomas-Hillman, J. Katrib, W. Lewis, C. Dodds, A. P. Harvey, S. W. Kingman, Combining continuous flow oscillatory baffled reactors and microwave heating: Process intensification and accelerated synthesis of metal-organic frameworks, Chemical Engineering Journal 356 (2019) 170–177.

[13] M. S. Lucas, N. M. Reis, G. L. Puma, Intensification of ozonation pro-

cesses in a novel , compact , multi-orifice oscillatory baffled column, Chemical Engineering Journal 296 (2016) 335–339.

[14] M. D. Soufi, B. Ghobadian, G. Naja, S. M. Mousavi, J. Aubin, Optimization of methyl ester production from waste cooking oil in a batch tri-orifice oscillatory baffled reactor, Fuel Processing Technology 167 (2017) 641–647.

[15] K. B. Smith, The Scale-Up of Oscillatory Flow Mixing, Ph.D. thesis, University of Cambridge (1999).

[16] D. González-Juárez, J. P. Solano, R. Herrero-Martín, A. P. Harvey, Residence time distribution in multiorifice baffled tubes: A numerical study, Chemical Engineering Research and Design 118 (2016) 259–269.

[17] X. Nogueira, B. J. Taylor, H. Gomez, I. Colominas, M. R. Mackley, Experimental and computational modeling of oscillatory flow within a baffled tube containing periodic-tri-orifice baffle geometries, Computers & Chemical Engineering 49 (2013) 1–17.

[18] J. Muñoz-Cámara, D. Crespí-Llorens, J. Solano, P. Vicente, Experimental analysis of flow pattern and heat transfer in circular-orifice baffled tubes, International Journal of Heat and Mass Transfer 147 (2020) 118914.

[19] Paste, Particle and Polymer Processing group (P4G), Oscillatory Fluid Mixing. OFM: Enhancement of heat transfer rates.
URL `https://www.ceb.cam.ac.uk/research/groups/rg-p4g/archiv`

e-folder/pfg/ofm-folder/ofm-advantages-enhancement-of-heat-transfer-rates

[20] G. G. Stephens, M. R. Mackley, Heat transfer performance for batch oscillatory flow mixing, Experimental Thermal and Fluid Science 25 (2002) 583–594.

[21] M.-S. Chae, B.-J. Chung, Laminar mixed-convection experiments in horizontal pipes and derivation of a semi-empirical buoyancy coefficient, International Journal of Thermal Sciences 84 (2014) 335–346.

[22] L. P. M. Colombo, A. Lucchini, A. Muzzio, Fully developed laminar mixed convection in uniformly heated horizontal annular ducts, International Journal of Thermal Sciences 94 (2015) 204–220.

[23] M. H. I. Baird, J. H. Garstang, Power consumption and gas hold-up in a pulsed column, Chemical Engineering Science 22 (12) (1967) 1663–1673.

[24] S. Churchill, H. Chu, Correlating Equations for Laminar and Turbulent Free Convection from a Horizontal Cylinder, International Journal of Heat Mass Transfer 18 (9) (1975) 1049–1053.

[25] B. S. Petukhov, Heat transfer and friction in turbulent pipe flow with variable physical properties, in: Advances in heat transfer, Vol. 6, Elsevier, 1970, pp. 503–564.

[26] J. P. Meyer, J. Olivier, Transitional flow inside enhanced tubes for fully developed and developing flow with different types of inlet disturbances : Part I Adiabatic pressure drops, International Journal of Heat and Mass Transfer 54 (2011) 1587–1597.

[27] M. Everts, J. P. Meyer, Heat transfer of developing and fully developed flow in smooth horizontal tubes in the transitional flow regime, International Journal of Heat and Mass Transfer 117 (2018) 1331–1351.

[28] J. P. Meyer, S. M. Abolarin, Heat transfer and pressure drop in the transitional flow regime for a smooth circular tube with twisted tape inserts and a square-edged inlet, International Journal of Heat and Mass Transfer 117 (2018) 11–29.

[29] G. Box, W. Hunter, J. Hunter, Statistics for Experimenters, 1978.

[30] D. Gedeon, J. G. Wood, Oscillating-Flow Regenerator Test Rig: Hardware and Theory With Derived Correlations for Screens and Felts, Tech. rep., NASA Contractor Report 198442 (1996).

[31] G. Xiao, H. Peng, H. Fan, U. Sultan, M. Ni, Characteristics of steady and oscillating flows through regenerator, International Journal of Heat and Mass Transfer 108 (2017) 309–321.

[32] R. Law, S. Ahmed, N. Tang, A. Phan, A. Harvey, Development of a more robust correlation for predicting heat transfer performance in oscillatory baffled reactors, Chemical Engineering and Processing: Process Intensification 125 (2018) 133–138.

[33] P. Stonestreet, P. M. J. van der Veeken, The effects of oscillatory flow and bulk fow components on residence time distribution in baffled tube reactors, Chemical Engineering Research and Design 77 (8) (1999) 671–684.